

Generation of Deep Ultraviolet Optical Vortices via Amplitude and Phase Spiral Zone Plates

A.S. Dyatlov,^{1,2,*} M.A. Nozdrin,² A.N. Sergeev,¹ N.E. Sheremet,¹ S.S. Stafeev,³ and D.V. Karlovets^{1,†}

¹*School of Physics and Engineering, ITMO University, 197101 St. Petersburg, Russia*

²*Joint Institute for Nuclear Research, 141980, Dubna, Russia*

³*Samara National Research University, 443086, Samara, Russia*

(Dated: January 31, 2025)

We present the development and experimental implementation of diffractive optical elements designed to generate optical vortices in the deep ultraviolet range (260–266 nm). These elements, fabricated using advanced lithographic and etching techniques, facilitate the efficient transformation of Gaussian beams into twisted modes carrying orbital angular momentum. Experimental tests conducted using the laser driver of an RF photoinjector at JINR successfully demonstrate the generation of deep-ultraviolet optical vortices with a topological charge of $l = 1$. These findings underscore the potential of structured light in the deep ultraviolet range for applications in relativistic electron beam studies and beam manipulation technologies.

I. INTRODUCTION

Vortex beams, characterized by their helical phase front rotating around the propagation axis and carrying orbital angular momentum (OAM) [1], constitute a distinct class of light and charged particle beams. These unique properties set them apart from Gaussian beams and have positioned the use of vortex beams as an innovative approach for exploring the quantum states of charged particles. Their applications have been extended to diverse fields, including telecommunications [2] and optical tweezer systems, which facilitate the precise manipulation of nanoscale objects [3] and many others [4].

In the case of charged particle beams, early studies primarily focused on systems limited to low energies, such as transmission or scanning electron microscopes (up to 300 keV) [5–7]. These facilities are also effectively self-contained and do not permit the particle beam for subsequent acceleration to relativistic and ultra-relativistic energies, despite the absence of any theoretical limitations for this [8]. To address this limitation, a project aimed at developing a source of relativistic electrons with a nonzero OAM was proposed. This initiative is a collaborative effort between the ITMO University and the Dzhelpev Laboratory of Nuclear Problems (DNLP) at the Joint Institute for Nuclear Research (JINR) [9].

The fundamental concept of this project involves the transfer of OAM from photons to electrons via photoemission. Theoretical studies have indicated that the OAM of a photon is almost nearly transferred to electrons during this process [10]. Consequently, the test facility for the RF photoinjector at Dzhelpev Laboratory has been modified. This test bench represents a classical RF photoinjector that incorporates a laser driver system, RF system, and accelerating structure represented by an RF gun developed by the Budker Institute of Nuclear

Physics [11]. The primary system requiring modification in this context is the laser driver of the JINR photoinjector. The laser driver was originally designed to work with photocathodes, which provide the highest quantum efficiency in the deep ultraviolet range, because the work function for an electron from the surface of such cathodes is in the region of 4-5 eV. [12]. However, this design imposes specific constraints on available methods for generating twisted photon beams. For example, spatial light modulators and digital micromirror devices cannot be employed, because their matrix structures cannot withstand high-power laser radiation, rendering them inoperable in this wavelength range. Studies on generating vortex beams at higher harmonics and transferring their states to the fourth harmonic have demonstrated a reduction in harmonic conversion efficiency [13], primarily because of the loss of linear polarization, which is a key requirement for maintaining phase-matching conditions. This reduction subsequently led to a significant decrease in photoelectron current.

An alternative concept for generating electron vortex beams involves magnetizing the cathode using a strong magnetic field [14]. This methodology also does not have the limitations associated with directing the beam to a target or high-frequency structures of the accelerator for further energy gain. However, this approach requires the creation of powerful fields near the cathode, and necessitates additional bunching and collimation of the electron beams after they are extracted from the source. In this regard, we primarily focused on the photoemission experiments.

Traditional methods have been employed to generate vortex beams to address this challenge. Among the existing techniques, spiral phase plates are notable because of their high conversion efficiency for light into vortex beams. However, the fabrication of spiral phase plates is challenging because of the intricate topology required on substrates, such as fused quartz or calcium fluoride (CaF_2), which remains underdeveloped. Another common method, fork diffraction grating, is simpler to fab-

* alexsandr.dyatlov@metalab.ifmo.ru

† dmitry.karlovets@metalab.ifmo.ru

ricate but exhibits suboptimal conversion efficiency and significant light intensity losses. Typically, the intensity of the incident beam is divided into three beams (two beams with and without the OAM), resulting in unavoidable losses.

To address these limitations, the development of spiral zone plates has been proposed. These plates offer the potential for high light conversion efficiency and are less complex to manufacture than spiral phase plates. The purpose of this study is to demonstrate the performance of the designed diffractive optical elements, evaluate their conversion efficiency into twisted optical modes, and validate the feasibility of generating such beams directly in the deep-ultraviolet range.

II. DESIGN AND MANUFACTURING

There are two primary types of spiral zone plate: amplitude and phase one [15, 16]. Amplitude zone plates modulate the light amplitude by utilizing alternating transparent and nontransparent spiral-shaped zones. The pattern of this configuration resulted in light diffraction and formation of a spiral wavefront. Their fabrication involves high-resolution patterning techniques, such as electron beam lithography, to ensure a precise zone structure and amplitude modulation.

In contrast, phase zone plates are designed to induce spatial variations in the light-beam phase while maintaining a relatively uniform amplitude. This is achieved through the incorporation of phase-shifting elements, such as grooves or microstructures, which modify the optical path length across the plate. The production of these devices requires precise control over the height and geometry of the structures, which can be accomplished using methods such as focused ion beam milling or nanoimprinting. These techniques ensure that the phase variations are smoothly distributed across the light wavefront, enabling manipulation of the phase profile of the beam.

In general, these plates are characterized by their ability to produce a phase shift that depends on both the angle and radius, effectively converting the incident light into vortex radiation. The functional form of the spiral zone plate can be expressed

$$SZP(r, \phi) = \exp\left(il\phi - \frac{i\pi r^2}{\lambda f}\right) \quad (1)$$

where (r, ϕ) denotes the polar coordinate system; l is the topological charge which equal to the OAM; λ is the operating wavelength of the light; f is the focal length for generating vortex beams. Upon binarization, Eq. 1 can be represented as a transfer function

$$T(r, \phi) = \begin{cases} 1, & \sin\left(l\phi - \frac{\pi r^2}{\lambda f}\right) \geq 0 \\ 0, & \sin\left(l\phi - \frac{\pi r^2}{\lambda f}\right) < 0 \end{cases} \quad (2)$$

where $T(r, \phi)$ represents the transfer function of the amplitude spiral zone plate mask. For the phase zone plate, the value of 0 on the right-hand side of the equation is replaced by -1 .

Figures 1 and 2 show the diffractive optical elements manufactured. For the amplitude zone plate, the mask was transferred onto a fused silica substrate using photolithography to achieve a resolution of up to $0.6 \mu\text{m}$. The diffraction pattern of the phase zone plate was transferred onto the substrate using photolithography, followed by the creation of a phase-modulating relief through plasma etching. A significant distinction between the produced phase and amplitude zone plates is that the focal length for vortex beam generation in the phase zone plate is one order of magnitude shorter, which allows fabrication with less stringent resolution requirements and simplifies the production process.

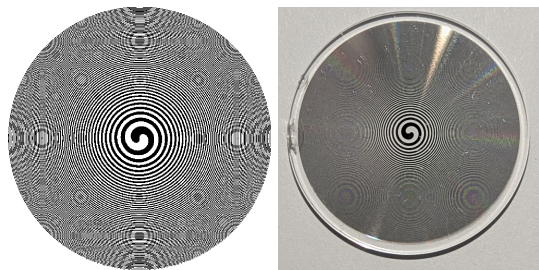


FIG. 1. Fabricated amplitude spiral zone plate. Left: amplitude mask; right: diffractive optical element

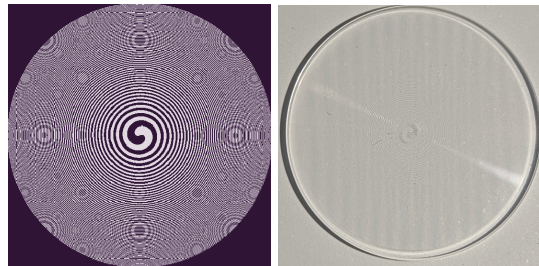


FIG. 2. Fabricated phase spiral zone plate. Left: phase mask; right: diffractive optical element

III. EXPERIMENTS AND RESULTS

The laser source for our experiment on the generation of deep ultraviolet optical vortices was the laser driver of the RF photoinjector at the DNLP JINR. This laser driver, developed by the Institute of Applied Physics of the Russian Academy of Sciences [17], is similar to those used in institutions such as DESY, KEK, and CERN [18]. A comprehensive schematic of the laser driver is shown in Figure 3 and the current parameters are listed in Table I.

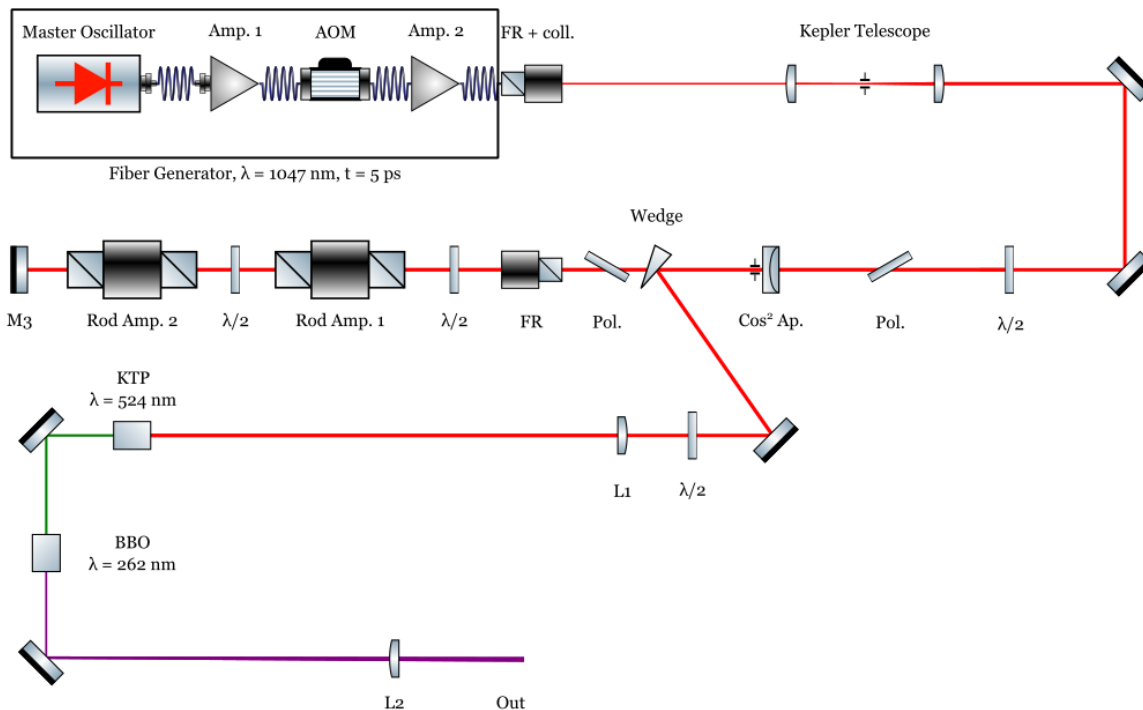


FIG. 3. Optical scheme of the DNLP JINR laser driver

Parameter	Value
Micropulse duration	10 ps
Micropulse repetition rate	40.225 MHz
Number of micropulse in burst	from 25 to 16000
Burst repetition rate	from 2 to 10 Hz
Wavelength	262 nm
Micropulse energy	3 – 4 μ J

TABLE I. Parameters of the DNLP JINR laser driver

The master oscillator is a fiber-based Yb-doped laser operating in a mode-locked regime, which generates radiation at the fundamental harmonic with a wavelength of $\lambda = 1047$ nm. Pulse trimming was accomplished using a semiconductor saturable-absorber mirror, resulting in a pulse duration of 5 ps.

The amplification section comprises two lamp-pumped Nd:YLF solid-state amplifiers, which increase the power of the infrared fundamental harmonic by approximately 80 times. After the amplification stage, a series of nonlinear crystals, including the KTP and BBO, were installed within the long beam waist of the telescope. These crystals generate the second and fourth harmonics, respectively.

The laser driver underwent further modifications in collaboration with the Institute of Applied Physics. The pulse repetition rate of the master oscillator is increased by adjusting the resonator length. This frequency was tuned to correspond to the 71st subharmonic of the accelerating RF power, which was 2856 MHz. In addition,

a system for controlling burst trimming was introduced, which enabled customizable burst lengths ranging from 25 to 16,000 micropulses. Because of these enhancements, the laser achieved a higher pulse energy, attaining 3–4 μ J per micropulse, compared to the initial design.

The experimental setup for generating optical vortices using spiral zone plates and determining the OAM of the generated beams is shown in Fig. 4. In our experiment, compensation for the astigmatism of the beam, which typically occurs after passing through the BBO crystal, was achieved by rotating a lens L_2 within the laser driver telescope system. This approach mitigates the need for additional corrections, which are a common requirement when lasers that generate higher harmonics are employed. The lens L_1 functions as an additional collimating element, because the divergence of the beam at the output of the laser driver remains relatively high.

Following collimation, a telescope system composed of lenses L_2 and L_3 was used to expand the beam further. This step was necessary because the working zones of the generated spiral zone plates were smaller than the beam size at the output of the DNLP JINR laser. After the beam expansion, the zone plates were sequentially integrated into the setup. This configuration of the laser driver is considered to be the primary one within the project for generating a source of relativistic electron vortices.

To measure the topological charge, we employed the mode converter introduced by Abramochkin in 1991 [19] and Beijersbergen in 1992 [20] which is widely used for

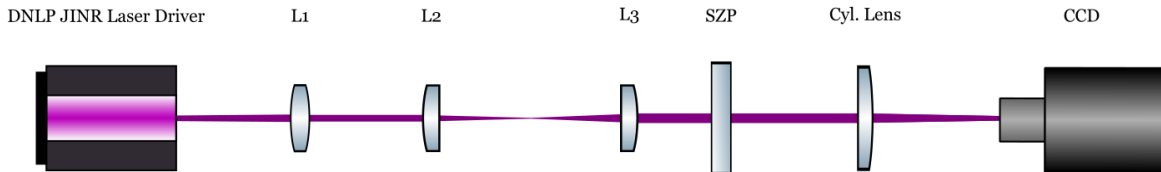


FIG. 4. Experimental scheme

generating optical vortices. In the original study, vortices were generated using two cylindrical lenses, collectively termed as the mode converter. These lenses enable the conversion of Laguerre-Gaussian modes of arbitrary order from Hermite-Gaussian modes by introducing a phase shift between the horizontal and vertical directions.

To obtain beams with nonzero angular momentum, a phase difference was introduced between the two vertical directions to facilitate the conversion from the Hermite-Gaussian to Laguerre-Gaussian modes. The classical converter consists of two identical cylindrical lenses placed at a distance $\sqrt{2}f$ for the $\pi/2$ -converter or $2f$ for the π -converter. A Laguerre-Gaussian mode with azimuthal index $l = n - m$ and radial index $p = \min(n, m)$ can be formed by passing the Hermite-Gaussian mode with indices m and n through the converter.

Conversely, reverse conversion from Laguerre-Gaussian to Hermite-Gaussian modes is also possible, allowing for numerical determination of the topological charge of optical vortices based on the order of the resulting Hermite-Gaussian mode of the beam. Furthermore, the topological charge can be numerically evaluated using a single cylindrical lens, although this leads to incomplete conversion, which causes the optical vortices to transform into a set of stripes. The number of stripes can be used to characterize the topological charge, as demonstrated by Kotlyar and Solomonov [21, 22]. This methodology was used to our experiments. After the beam-expanding telescope, spiral zone plate elements were introduced into the setup. The resulting beam was then directed toward a cylindrical lens. A CCD camera was placed on the focal plane of the lens to visualize spatial profiles.

The primary instrument used to visualize the obtained modes was an SDU-285R CCD camera manufactured by “SpetsTeleTechnika” LLC. This camera was equipped with a SONY ICX285AL CCD matrix with a resolution of 1392×1032 pixels and pixel size of $6.45 \times 6.45 \mu\text{m}$. To enhance the sensitivity to deep ultraviolet light, the camera was modified by removing the protective glass from the matrix, thereby eliminating the scattering and absorption of the deep ultraviolet light. This modification enabled the visualization of beams in this wavelength range. The spatial profiles of the beams obtained during the experiment are presented in Figures 5 and 6. For improved contrast and a clearer identification of the con-

verted mode order, the image on the right in the provided figures was recorded in “Color Mode.”

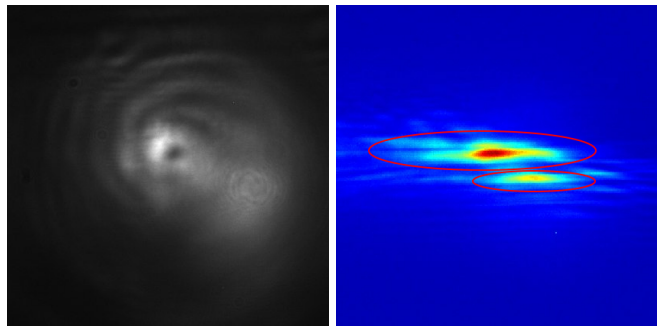


FIG. 5. Spatial profiles obtained from diffraction on the amplitude spiral zone plate. Left: optical vortices; Right: converted mode obtained after the vortex beam passes through the cylindrical lens. The topological charge is defined as the number of fringes minus one.

Figure 5 illustrates the spatial profiles obtained from the diffraction of the amplitude spiral zone plate. As observed in the left panel, the quality of the transformation is suboptimal, as indicated by Fourier analysis [15]. This imperfection stems from the low efficiency of the amplitude plate, which is approximately 10% that of the incident light. This low efficiency is also clear in mode conversion, as shown in the right panel. The two fringes obtained during the mode conversion correspond to an initial beam with a topological charge of $l = 1$. However, the fringes were inhomogeneous, albeit clearly visible.

Figure 6 shows the spatial profiles obtained by diffraction in the phase spiral zone plate. As anticipated, owing to the phase modulation of light, the efficiency of transforming the Gaussian beam into a Laguerre-Gaussian beam was higher than that of the amplitude plate by approximately 40%. Furthermore, the amount of optical noise is significantly lower than that in the first case. This is also reflected in the mode conversion: the right panel exhibits more uniform fringes, which closely align with the expected results. The number of fringes corresponds to a topological charge of $l = 1$, indicating the overall efficiency of the generation of optical vortices by both spiral zone plates.

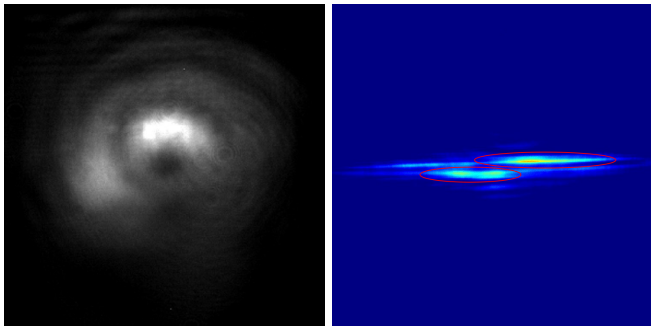


FIG. 6. Spatial profiles obtained from diffraction on the phase spiral zone plate. Left: optical vortices; Right: converted mode obtained after the vortex beam passes through the cylindrical lens. The topological charge is defined as the number of fringes minus one.

IV. DISCUSSION

We have demonstrated the functionality of diffractive optical elements in the deep ultraviolet light range. While achieving efficient optical vortex generation, further improvements are possible by refining the fabrication of spiral zone plates, particularly by reducing the mask period. This modification is expected to enhance the quality of the optical vortex beams, which will positively impact the generation of electron beams.

Increasing the OAM of optical beams is another promising avenue for advancing this technology, because it enables electron beams with a greater OAM. Alternative optical vortex-generating elements, including diffraction fork gratings and spiral phase plates, have also been explored. Spiral phase plates are anticipated to exhibit the highest efficiency [23] owing to their superior phase-modulating properties, as demonstrated in phase zone plate experiments. However, their complex surface topology significantly complicates the fabrication process and

presents a key challenge for their implementation.

Previous studies on deep ultraviolet vortex generation have primarily focused on producing second-harmonic beams and transferring their state to the fourth harmonic [13]. Although this approach can be adapted to the current system, it suffers from a low harmonic conversion efficiency owing to disrupted polarization in the vortex beams. This limitation reduces the quantum efficiency of photoelectron generation, thereby hindering the collection of statistically significant data for the analysis.

The laser system developed in this study for generating optical vortex beams integrates effectively with the RF photoinjector at the DNLP JINR, forming a robust foundation for future experiments aimed at generating electron vortices. This system represents a significant step toward expanding the potential of optical vortex technologies in practical applications.

These advancements will not only improve the efficiency of deep ultraviolet vortex generation systems but also enable broader applications in accelerator physics and quantum research. Enhanced vortex electron beams are expected to support advanced experiments on particle manipulation, beam diagnostics, and quantum state control. Ultimately, our approach promises significant benefits for both fundamental and large-scale scientific research.

ACKNOWLEDGEMENT

We sincerely thank K. Cherepanov for his invaluable assistance and advice. We are also grateful to S. Baturin for the helpful discussions and constructive feedback. Special thanks to the Institute of Applied Physics of the Russian Academy of Sciences and M. Martyanov for rebuilding the laser driver and for their continued support in restoring it. This study was supported by the Russian Science Foundation (Project No. 23-62-10026) [9].

-
- [1] L. Allen, M. W. Beijersbergen, R. J. C. Spreeuw, and J. P. Woerdman, Orbital angular momentum of light and the transformation of laguerre-gaussian laser modes, *Phys. Rev. A* **45**, 8185 (1992).
 - [2] M. Mirhosseini, O. S. Magaña-Loaiza, M. N. O’Sullivan, B. Rodenburg, M. Malik, M. P. J. Lavery, M. J. Padgett, D. J. Gauthier, and R. W. Boyd, High-dimensional quantum cryptography with twisted light, *New Journal of Physics* **17**, 033033 (2015).
 - [3] F. M. Muñoz-Pérez, V. Ferrando, W. D. Furlan, J. C. Castro-Palacio, J. R. Arias-Gonzalez, and J. A. Monsoriu, Multiplexed vortex beam-based optical tweezers generated with spiral phase mask, *iScience* **26**, 107987 (2023).
 - [4] H. Rubinsztein-Dunlop, A. Forbes, M. V. Berry, M. R. Dennis, D. L. Andrews, M. Mansuripur, C. Denz, C. Alpmann, P. Banzer, T. Bauer, E. Karimi, L. Marrucci, M. Padgett, M. Ritsch-Marte, N. M. Litchinitser, N. P. Bigelow, C. Rosales-Guzmán, A. Belmonte, J. P. Torres, T. W. Neely, M. Baker, R. Gordon, A. B. Stilgoe, J. Romero, A. G. White, R. Fickler, A. E. Willner, G. Xie, B. McMorran, and A. M. Weiner, Roadmap on structured light, *Journal of Optics* **19**, 013001 (2016).
 - [5] M. Uchida and A. Tonomura, Generation of electron beams carrying orbital angular momentum, *Nature* **464**, 737– (2010).
 - [6] J. Verbeeck, H. Tian, and P. Schattschneider, Production and application of electron vortex beams, *Nature* **467**, 301 (2010).
 - [7] A. Blackburn and J. Loudon, Vortex beam production and contrast enhancement from a magnetic spiral phase plate, *Ultramicroscopy* **136**, 127 (2014).
 - [8] D. Karlovets, Vortex particles in axially symmetric fields and applications of the quantum busch theorem, *New*

- Journal of Physics **23**, 033048 (2021).
- [9] <https://rscf.ru/en/project/23-62-10026/>.
- [10] I. I. Pavlov, A. D. Chaikovskaia, and D. V. Karlovets, Generation of vortex electrons by atomic photoionization, Phys. Rev. A **110**, L031101 (2024).
- [11] D. A. Nikiforov, A. E. Levichev, A. M. Barnyakov, A. V. Andrianov, and S. L. Samoilo, Simulation of a radio-frequency photogun for the generation of ultrashort beams, Electrophysics, Electron and Ion Beams, Physics of Accelerators **63**, 585 (2018).
- [12] R. Xiang and J. Teichert, Photocathodes for high brightness photo injectors, Physics Procedia **77**, 58 (2015), international Conference on Laser Applications at Accelerators, LA3NET 2015, 25-27 March 2015, Mallorca, Spain.
- [13] Y. Sasaki, M. Koyama, K. Miyamoto, Y. Ariga, T. Onda, I. Shoji, and T. Omatsu, Ultraviolet vortex generation using periodically bonded β -bab2o4 device, Opt. Express **22**, 12829 (2014).
- [14] K. Floettmann and D. Karlovets, Quantum mechanical formulation of the busch theorem, Phys. Rev. A **102**, 043517 (2020).
- [15] M. K. Sharma, R. K. Singh, J. Joseph, and P. Senthil Kumaran, Fourier spectrum analysis of spiral zone plates, Optics Communications **304**, 43 (2013).
- [16] E. S. Kozlova and V. V. Kotlyar, Comparative simulation of spiral zone plates with a relief from silica glass and silver, Journal of Physics: Conference Series **1368**, 022020 (2019).
- [17] E. I. Gacheva, A. K. Poteomkin, E. A. Khazanov, V. V. Zelenogorskii, E. V. Katin, G. A. Luchinin, N. I. Bala-lykin, V. F. Minashkin, M. A. Nozdrin, G. V. Trubnikov, and G. D. Shirkov, Laser driver for a photoinjector of an electron linear accelerator (february 2014), IEEE Journal of Quantum Electronics **50**, 522 (2014).
- [18] I. Will and G. Klemz, Drive lasers for photoinjectors, in *ERL07* (2007).
- [19] E. Abramochkin and V. Volostnikov, Beam transformations and nontransformed beams, Optics Communications **83**, 123 (1991).
- [20] M. Beijersbergen, L. Allen, H. van der Veen, and J. Woerdman, Astigmatic laser mode converters and transfer of orbital angular momentum, Optics Communications **96**, 123 (1993).
- [21] V. V. Kotlyar, A. A. Kovalev, and A. P. Porfirev, Astigmatic transforms of an optical vortex for measurement of its topological charge, Appl. Opt. **56**, 4095 (2017).
- [22] A. I. Solomonov, O. M. Kushchenko, K. I. Kasyanova, S. B. Isaeva, I. I. Shishkin, D. Y. Terekhov, P. I. Lazarenko, M. V. Rybin, S. S. Baturin, and A. D. Sinelnik, Switching topological charge of optical vortex by two-dimensional structures, Applied Materials Today **37**, 102135 (2024).
- [23] M. Massari, G. Ruffato, M. Gintoli, F. Ricci, and F. Romanato, Fabrication and characterization of high-quality spiral phase plates for optical applications, Appl. Opt. **54**, 4077 (2015).